

# Detailed neutron diffraction study of magnetic order in NdFe<sub>2</sub>Al<sub>10</sub>

Julien Robert,<sup>1</sup> Françoise Damay,<sup>1</sup> Kotaro Saito,<sup>1,\*</sup> Alexandre M. Bataille,<sup>1</sup> Florence Porcher,<sup>1</sup> Gilles André,<sup>1</sup> Arsen Gukasov,<sup>1</sup> Jean-Michel Mignot,<sup>1,†</sup> Hiroshi Tanida,<sup>2</sup> and Masafumi Sera<sup>2</sup>

<sup>1</sup>Laboratoire Léon Brillouin, CEA-CNRS, CEA/Saclay, 91191 Gif sur Yvette, France

<sup>2</sup>Department of Quantum Matter, ADSM, Hiroshima University, Higashi-Hiroshima, 739-8530, Japan

(Dated: December 7, 2024)

The compound NdFe<sub>2</sub>Al<sub>10</sub> (*Cmcm*, space group #63) has been studied by both powder and single-crystal neutron diffraction. Below  $T_N = 3.9$  K, the Nd<sup>3+</sup> magnetic moments order in a commensurate magnetic structure, whose unit cell consists of four orthorhombic unit cells stacked along the *b* direction. It can be described either as double- $\mathbf{k}$  [ $\mathbf{k}_1 = (0, \frac{1}{4}, 0)$ ], [ $\mathbf{k}_3 = (0, \frac{3}{4}, 0)$ ] on the original base-centered orthorhombic lattice or, equivalently, as single- $\mathbf{k}$  (wave vector  $\mathbf{k}_1$  alone) on the primitive orthorhombic lattice obtained by considering corners and centers of (0 0 1) faces as inequivalent. The intensity refinements point to a structure consisting of (0 1 0) ferromagnetic planes stacked along the *b* direction, in which the moments are collinear and oriented along the *a* axis (easy direction according to bulk magnetization measurements). The alternating sequence providing the best refinement turns out to be that which yields the lowest exchange energy if one assumes antiferromagnetic near-neighbor exchange interactions with  $J_1 \gg J_2, J_3$ . Information is also presented regarding the temperature and magnetic field dependence of the magnetic structure.

PACS numbers: 71.27.+a, 71.70.Ch, 71.70.Gm, 75.25.+z, 75.30.Gw, 75.30.Kz,

Keywords: NdFe<sub>2</sub>Al<sub>10</sub>, neutron powder diffraction, single-crystal neutron diffraction, magnetic structure, commensurate order, discommensuration, magnetic field

## I. INTRODUCTION

Orthorhombic compounds with formula CeT<sub>2</sub>Al<sub>10</sub> with *T*: Ru, Os, Fe have attracted considerable interest recently because they exhibit a very peculiar coexistence of long-range magnetic order and Kondo-insulator properties,<sup>1–3</sup> which has been ascribed to an unusually strong anisotropy of the hybridization between 4*f* and conduction electron states.<sup>4,5</sup> The antiferromagnetic (AFM) order reported for CeRu<sub>2</sub>Al<sub>10</sub> and CeOs<sub>2</sub>Al<sub>10</sub> in itself has a number of intriguing features such as the very large value of the ordering temperature  $T_0 = 27$  K in comparison with other RT<sub>2</sub>Al<sub>10</sub> compounds (*R*: Nd, Gd),<sup>6,7</sup> the direction of the AFM moment ( $\mathbf{m}_{\text{AF}} \parallel c$ ) not complying with the single-ion anisotropy (easy *a* axis), or the lack of transverse (“ $\chi_{\perp}$ ”-type) behavior in the temperature dependence of the magnetic susceptibility  $\chi_a(T)$  for a field applied along  $a \perp \mathbf{m}_{\text{AF}}$ , etc. Neutron scattering experiments have clarified several aspects of the magnetic structure<sup>8–10</sup> (AFM with propagation vector  $\mathbf{k} = (0, 1, 0)$  and a strongly reduced Ce magnetic moment, on the order of 0.3  $\mu_B$ ) and dynamics<sup>8,9,11</sup> (spin gap and dispersive magnetic excitations forming below  $T_0$ ). The spectrum of magnetic excitations, in particular, points to a strong anisotropy of exchange interactions, which competes with the conventional crystal-field anisotropy.

In an attempt to set an appropriate reference for the exotic magnetism occurring in the Ce compounds, experiments have been carried out on their Nd counterparts, which are likely to exhibit “normal-rare-earth” properties, amenable to a standard description in terms of crystal-field (CF) and Ruderman-Kittel-Kasuya-Yosida (RKKY) exchange interactions. The results reported by

Kunimori *et al.*<sup>7</sup> confirmed this expectation by showing that the anisotropic magnetization (easy *a* axis) in the paramagnetic regime can be reproduced satisfactorily using a simple two-sublattice mean-field model, with a small CF splitting, imputable to the large distance from the Ce ion to its ligands, and a moderate anisotropy in the exchange interactions. Below the ordering temperature  $T_N = 3.9$  K, the ordered moment is oriented along the easy anisotropy axis, and its magnitude looks consistent with the values expected for the Nd<sup>3+</sup> CF doublet ground state. The overall picture is thus that of weakly interacting integral-valence rare-earth ions.

In the present work we have performed neutron diffraction experiments to characterize the magnetic structure of NdFe<sub>2</sub>Al<sub>10</sub>, which could not be determined from magnetic measurements alone. This structure is found to be commensurate with cell dimensions  $a \times 4b \times c$ , and can be derived from the AFM structure of CeRu<sub>2</sub>Al<sub>10</sub> and CeOs<sub>2</sub>Al<sub>10</sub> by a change in the moment direction and the introduction of discommensurations.

## II. EXPERIMENTS

NdFe<sub>2</sub>Al<sub>10</sub> was synthesized in single-crystal form starting from 99.9% Nd and 99.995% Fe constituents in a 99.999% Al flux. A powder sample of 6.3 g in mass was prepared by crushing small single-crystal pieces. Neutron powder diffraction (NPD) patterns were collected on the two-axis diffractometer G4-1 (Orphée-LLB, Saclay) equipped with a 800-cell position-sensitive detector. A monochromatic incident neutron beam of wavelength  $\lambda_i = 2.426$  Å was produced by a pyrolytic graphite (PG002) monochromator, and higher-order contamina-

TABLE I. Nuclear structure parameters of NdFe<sub>2</sub>Al<sub>10</sub> at room temperature.

	Space group	$a_0$ (Å)	$b_0$ (Å)	$c_0$ (Å)	$R$ factor	$\chi^2$
this work	$Cmcm$	9.0148(7)	10.2168(7)	9.0793(7)	3.31	2.89
x-rays (Ref. 12)	$Cmcm$	9.0158(1)	10.2182(1)	9.0800(1)		

	$y_{Nd}$	$x_{Al(1)}$	$y_{Al(1)}$	$x_{Al(2)}$	$y_{Al(2)}$	$y_{Al(3)}$	$z_{Al(3)}$	$y_{Al(4)}$	$z_{Al(4)}$	$x_{Al(5)}$
this work	0.1238	0.2290	0.3617	0.3500	0.1286	0.1602	0.5975	0.3765	0.0514	0.2280
x-rays (Ref. 12)	0.12428	0.22727	0.36085	0.34989	0.12843	0.16077	0.59844	0.37661	0.05077	0.22721

tion was suppressed by means of a PG filter. The sample powder was contained in a thin-walled cylinder-shape vanadium container, 6 mm in diameter, and cooled to 1.7 K in the exchange-gas chamber of a liquid-He cryostat. The data analysis was performed using the Rietveld refinement program FULLPROF,<sup>13,14</sup> with neutron scattering lengths and magnetic form factors taken from Refs. 15 and 16, respectively. Absorption corrections were treated as negligible.

A large single-crystal ( $m = 0.201$  g) was mounted on an aluminum sample holder with the  $a$  axis vertical, and cooled to 1.7 K in the variable-temperature insert (VTI) of a 7-T, split-coil, vertical-field cryomagnet from Oxford Instruments. Single-crystal diffraction (SCD) experiments were performed on the thermal beam, two-axis neutron diffractometer Super-6T2 (Orphée-LLB).<sup>17</sup> Intensity maps were measured at two incident wavelengths,  $\lambda_i = 0.902$  Å (Cu monochromator, Er filter) and 2.345 Å (PG002 monochromator, PG filter), by rotating the sample around the vertical axis with 0.1° steps and recording the diffraction pattern in a BIDIM26 multiwire position-sensitive gas detector (PSD) developed at the ILL (Grenoble) and manufactured by INEL (Artenay, France). This procedure allowed us to explore a large three-dimensional (3D) segment of the reciprocal space by transforming a complete set of PSD images into the reciprocal space of the crystal. For quantitative refinements and studies of temperature and magnetic field dependences, the configuration was changed to a single lifting counter, with 20' Soller collimators. An extensive data set was collected at  $\lambda_i = 0.902$  Å in zero field at the base temperature, and more restricted ones at  $T = 2.7$  K and at  $H = 2.6$  T. The results were analyzed using the Cambridge Crystallography Subroutine Library (CCSL).<sup>18</sup>

### III. RESULTS

#### A. Crystal structure

The room-temperature (RT) crystal structure was first checked on the high-resolution powder diffractometer 3T2 (Orphée-LLB), using an incident neutron wavelength  $\lambda_i = 1.2251(2)$  Å. The diffraction pattern is shown in Fig. 1. The parameters derived from the Rietveld refinement, listed in Table I, are in excellent agreement

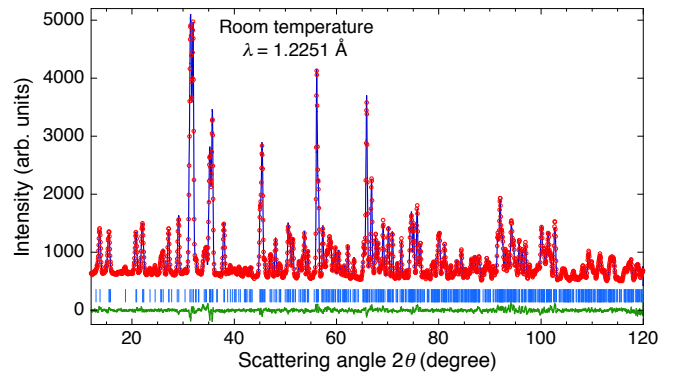


FIG. 1. (Color online) Rietveld refinement of the high-resolution neutron-diffraction pattern of NdFe<sub>2</sub>Al<sub>10</sub> measured on 3T2 at room temperature. Open circles: measured intensities; full line through data: refinement; vertical marks: position of Bragg reflections; bottom trace: difference between measured and calculated intensities.

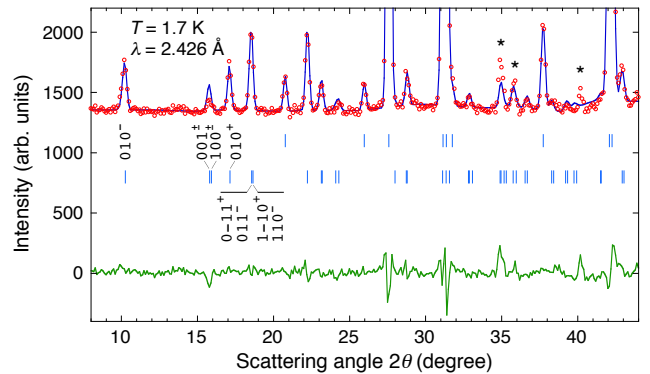


FIG. 2. (Color online) Rietveld refinement of the neutron-diffraction pattern of NdFe<sub>2</sub>Al<sub>10</sub> measured on G4-1 at  $T = 1.7$  K. Open circles: measured intensities; full line through data: refinement; vertical marks: position of Bragg reflections; bottom trace: difference between measured and calculated intensities; Stars signal positions at which contamination by a nonmagnetic impurity is observed for  $T > T_N$ .

with the space group, lattice constants,<sup>12,19</sup> and atomic parameters<sup>12</sup> determined previously by x-ray diffraction.

## B. Magnetic structure: powder diffraction

The NPD pattern measured on G4-1 for  $T = 1.7$  K is presented in Fig. 2. Magnetic superstructure peaks are clearly visible at low scattering angles. However, these peaks cannot be indexed in the original  $Cmcm$  space group using a single  $\mathbf{k}$  vector. The reason, made obvious from the positions of the Bragg spots in the single-crystal map to be discussed in the following, is that  $\pm\mathbf{k}$  satellites occur not only at the positions of the allowed nuclear reflections but also, with even larger intensities, at positions which are forbidden by the centering of the unit cell. If one simply relaxes this extra condition and treats the magnetic superstructure in the primitive orthorhombic lattice, then all satellites can be indexed using the single propagation vector  $\mathbf{k}_1 = (0, \frac{1}{4}, 0)$ .

On the other hand, the nuclear reflections measured in the same temperature range give no indication of a symmetry lowering with respect to the  $Cmcm$  space group assigned from accurate x-ray diffraction measurements at room temperature,<sup>12,19</sup> and confirmed on the present sample by the neutron data from 3T2 (Sect. III A). In fact, it turns out that an alternative description of the same diffraction pattern can be achieved within the original space group, provided one introduces a second wave vector  $\mathbf{k}_3 = 3\mathbf{k}_1 = (0, \frac{3}{4}, 0)$ . Formally, this vector can be regarded as a third harmonic of  $\mathbf{k}_1$  but, unlike the case of modulated structures exhibiting gradual squaring as temperature goes to zero, here the magnitude  $m_2$  of the Fourier component associated with  $\mathbf{k}_3$  largely exceeds the value  $\frac{1}{3}m_1$  corresponding to a fully squared modulation. In the following, the single- $\mathbf{k}$  notation within the primitive space group will be used for convenience when referring to particular reflections. For instance,  $100^+$  (rather than  $110^{3-}$ ) will denote the peak measured at  $\mathbf{Q} = (1, 0.25, 0)$ , although 100 does not fulfill the  $h + k = 2n$  reflection condition of the  $Cmcm$  space group.

Because the diffraction pattern was measured at  $T = 1.7$  K  $\approx 0.4T_N$ , we have supposed that the structure consists of saturated Nd magnetic moments of *equal size*, which means, for the particular value of  $\mathbf{k}_1 = (0, \frac{1}{4}, 0)$  (in the primitive description), four “+ + - -” sequences propagating along  $b$  on four independent  $P$  sublattices. Indirect support for this assumption comes from the fact that it provides a natural explanation for the existence of a second  $\mathbf{k}$  vector in the  $C$  description—or the decoupling of “base-center” and “base-corner” sites in the  $P$  description: this condition is necessary for constant-moment solutions to exist with a periodicity of 4 unit cells along the  $b$  direction.

We have carried out a systematic investigation of all possible phase relationships between the four magnetic sublattices that produce constant moments at the Nd sites and no net magnetization. From a total of 256, only 24 correspond to distinct magnetic structures, for which FULLPROF refinements were performed. The best fit, represented by the solid line in Fig. 2, has a magnetic  $R$ -

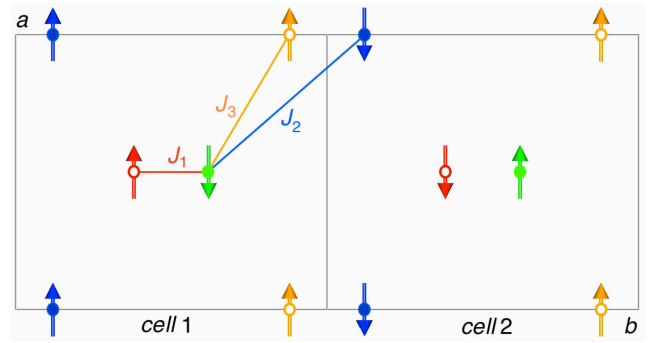


FIG. 3. (Color online) Schematic representation of the magnetic structure yielding the best Rietveld refinement of the NPD data at  $T = 1.7$  K (see text). Arrows parallel to the  $a$  axis represent Nd magnetic moments located in the  $z = \frac{1}{4}$  (blue, green : closed circles) and  $z = \frac{3}{4}$  (red, orange : open circles) planes, respectively. Moments in cells 3 and 4 (not shown) are antiparallel to those in cells 1 and 2, respectively.  $J_1$ ,  $J_2$ , and  $J_3$  denote exchange interactions between Nd near neighbors, as discussed in Sect. IV.

factor of 19 (24) excluding (including) the contaminated regions denoted by stars in Fig. 2, and corresponds to the collinear structure represented in Fig. 3 with Nd moments of  $1.75(4) \mu_B$ . The  $b^*$  component of the  $\mathbf{k}$  vector refines to 0.2497 r.l.u., i.e.  $\frac{1}{4}$  within experimental accuracy. The only visible disagreement (apart from the contaminations near  $2\theta = 35$  and  $40^\circ$ , which already exist above  $T_N$  and up to RT) is some overestimation of the intensity of the  $001^\pm$  and/or  $100^\pm$  magnetic satellites.

The refinement is very sensitive to the orientation of the moments, which are unambiguously parallel to the easy  $a$  axis, as was inferred earlier from the bulk magnetization measurements.<sup>7</sup> The magnetic  $R$ -factor for the next best solution is 33 (36), indicating that the agreement with the experimental data is significantly worse (it completely fails, e.g., to account for the strong intensity of the  $010^-$  peak near  $2\theta = 10^\circ$ ). Relaxing the condition of equal moments at all sites, i.e. allowing solutions with moment amplitude modulations, did not yield meaningful improvement [ $R$ -factor = 18 (21)].

With increasing temperature, the magnetic signal decreases gradually and the refinements lead to the temperature dependence of the Nd magnetic moment plotted in Fig. 4, which vanishes above the Néel temperature  $T_N = 3.9$  K. Surprisingly, no indication of a change in the magnetic structure could be observed near the temperature of 2.3 K, at which anomalies were observed in specific heat,<sup>7</sup>  $\mu$ SR,<sup>20</sup> and electrical resistivity<sup>21</sup> measurements.

## C. Magnetic structure: single-crystal diffraction

Figure 5(a) shows a cut in the  $h = 0$  plane in reciprocal space measured at  $T = 1.7$  K with an incident wavelength  $\lambda_i = 2.345$  Å using the PSD on 6T2. The nuclear peaks are observed at the positions ( $k$  even,  $l$  even if  $k = 0$ )

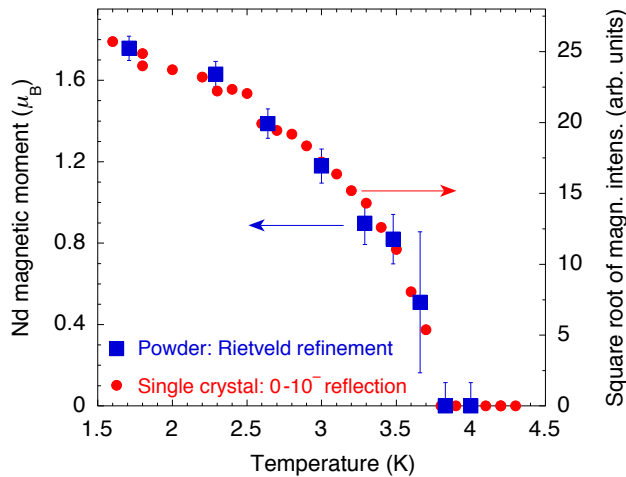


FIG. 4. (Color online) Temperature dependence of the magnetic diffraction component in  $\text{NdFe}_2\text{Al}_{10}$ . Closed squares (left scale): Nd magnetic moment obtained from the Rietveld refinements of the NPD patterns using the magnetic structure described in the text. Closed circles (right scale): square root of the integrated intensity of the  $0\bar{1}0^-$  satellite [ $Q = (0, -\frac{5}{4}, 0)$ ]. The vertical scales have been adjusted to emphasize the similarity of the temperature variations.

corresponding to the reflection conditions for the  $Cmcm$  space group, namely:  $h+k = 2n$ , with  $h+l = 2n$  if  $k = 0$ . The violation observed in  $00\bar{1}$  is ascribed to multiple scattering. Satellites are clearly visible at positions shifted by  $\pm\frac{1}{4}\mathbf{b}^*$  from nuclear peaks. However, even stronger magnetic reflections exist near some of the extinct positions (e.g.  $01\bar{3}^\pm$ ). As mentioned in Sect. III B, these satellites can still be indexed in the  $Cmcm$  space group (two  $oC$  Nd Bravais lattices) by adding the second wave vector  $\mathbf{k}_3 = (0, \frac{3}{4}, 0)$ , although the primitive orthorhombic description (four  $oP$  Nd Bravais lattices) can be adopted for convenience in the calculations.

To study the higher layers  $h = 1$  and  $2$ , it was necessary to use a shorter wavelength  $\lambda_i = 0.902 \text{ \AA}$  with the Cu monochromator to remain within the solid angle covered by the detector and the vertical opening of the cryomagnet. The maps measured at  $T = 1.7 \text{ K}$  for  $h = 1$  and  $2$  are shown in Figs. 5(b) and (c) (for  $h = 0$ , the results are consistent with those of Fig. 5(a), but only the stronger  $\mathbf{k}_3$  satellites can be detected). The map for  $h = 2$  is qualitatively similar to that for  $h = 0$ , but few satellites remain observable. For  $h = 1$  reflection conditions reduce to:  $k$  odd. Again, the stronger  $\mathbf{k}_3$  satellites occur near forbidden ( $k = 2n$ ) reciprocal lattice points. These observations are fully consistent with the magnetic structure suggested from the NPD results.

Measurements performed using the lifting counter further confirm the validity of this solution. The  $(0, k, 3)$  longitudinal scan along the  $b^*$  direction presented in Figure 6 demonstrates that the  $b^*$  component of the  $\mathbf{k}$  vector is locked at the commensurate value  $\frac{1}{4}$ . The integrated intensities of 178 nonequivalent magnetic reflections have

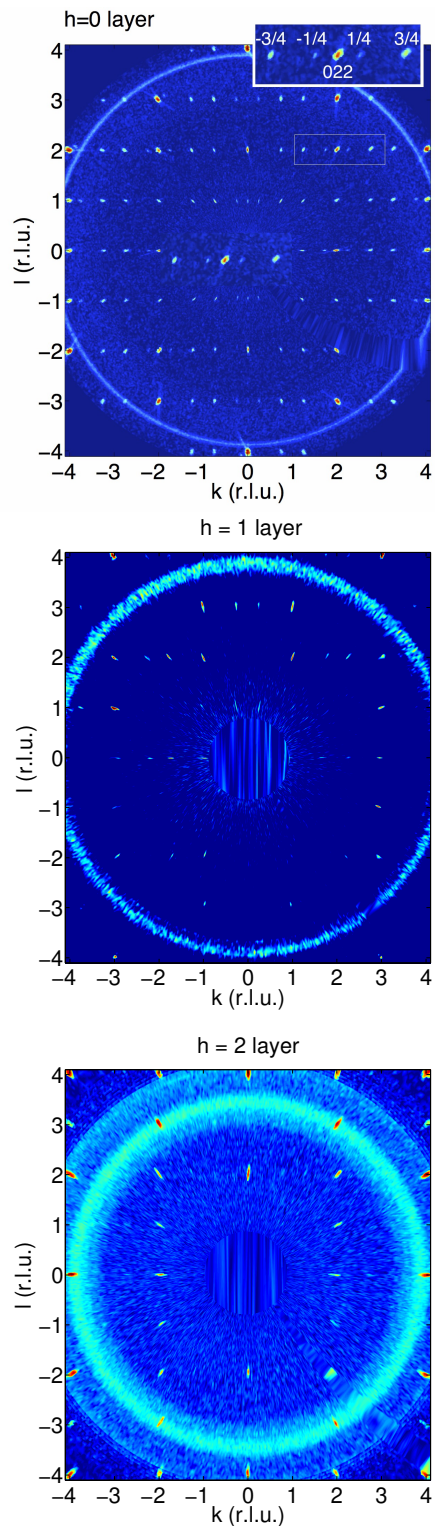


FIG. 5. (Color online) Diffraction maps on  $\text{NdFe}_2\text{Al}_{10}$  in the  $(0, k, l)$  (upper frame),  $(1, k, l)$  (middle frame), and  $(2, k, l)$  (lower frame) planes in reciprocal space, obtained from the PSD measurements on Super-6T2. The incident neutron wavelength was  $\lambda_i = 2.345 \text{ \AA}$  (PG monochromator) for  $h = 0$  and  $\lambda_i = 0.902 \text{ \AA}$  (Cu monochromator) for  $h = 1$  and  $2$ .



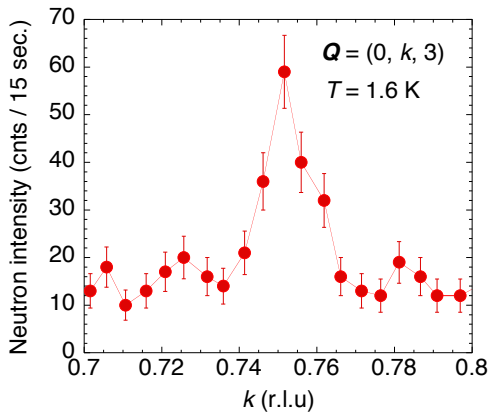


FIG. 6. (Color online) Longitudinal profile of the  $013^-$  satellite [ $\mathbf{Q} = (0, \frac{3}{4}, 0)$ ] measured at  $T = 1.6$  K.

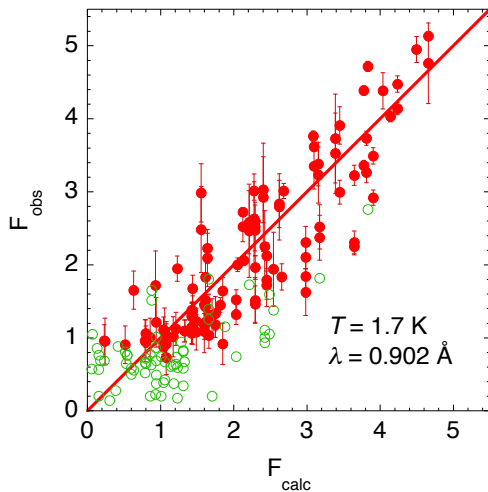


FIG. 7. (Color online) Linear correlation between the experimental magnetic structure factors (square root of the measured integrated intensities divided by the Lorentz factor) for 178 magnetic reflections and the values calculated for the magnetic structure described in the text and shown in Fig. 3 (component perpendicular to  $\mathbf{Q}$ , corrected for extinction). Closed red (open green) markers denote reflections whose measured  $F_{\text{obs}}$  are larger (smaller) than 3 times their standard deviations.

been collected at the base temperature of 1.7 K by performing rocking curves through the nominal peak positions. Figure 7 shows that there is a good linear correlation between the measured  $F_{\text{obs}}$  (square root of the intensity corrected for the Lorentz factor) and  $F_{\text{calc}}$ , the component normal to the scattering vector of the calculated magnetic structure factor (including the magnetic form factor and corrected for extinction effects). The refinement has a reliability factor of 16% (all reflections included), and yields an ordered magnetic moment of  $1.95(7) \mu_B$  on the Nd ions, slightly larger than that obtained in the NPD measurements.

In Fig. 4, the square root of the integrated intensity

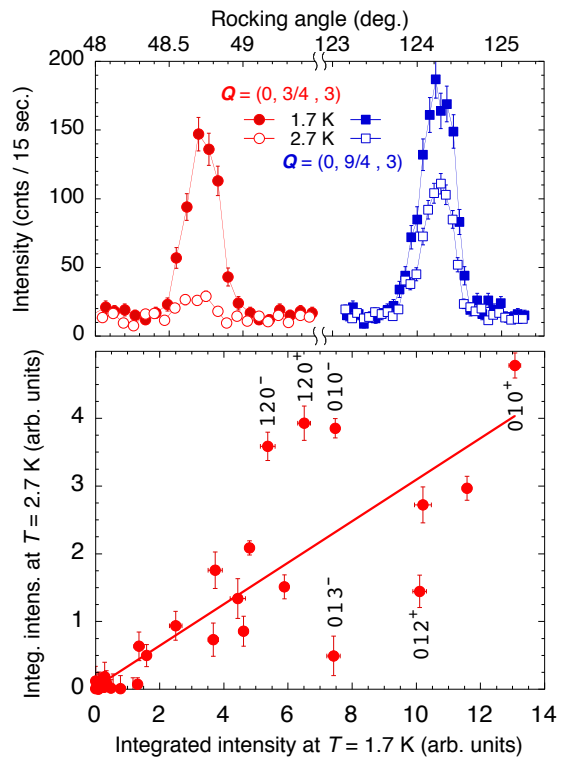


FIG. 8. (Color online) Temperature evolution of the magnetic Bragg intensities between 1.7 and 2.7 K, revealing non-uniform behaviors amongst the 33 reflections studied. Contrasting examples of rocking curves are shown in the upper frame for the  $013^-$  and  $023^+$  reflections.

of the  $0\frac{3}{4}0$  magnetic reflection is shown to follow the temperature dependence of the Nd magnetic moment derived from the Rietveld refinements of the powder data (Sect. III B). Despite the much smaller temperature step used here, in comparison with the NPD data (Sect. III B), there is still no clear evidence for the second transition expected to occur near 2.5 K.

However, more careful examination of the temperature dependence of a representative set of magnetic reflections indeed reveals that their integrated intensities do not change by the same ratio between 1.7 K and 2.7 K. As can be seen in Fig. 8, some peaks exhibit significant (either positive or negative) deviations with respect to the general intensity decrease occurring as temperature goes up. This observation suggests that a minor change in the magnetic structure may take place near 2.5 K in connection with the anomaly observed in other physical properties, even though the  $\mathbf{k}$ -vectors  $\mathbf{k}_1$  and  $\mathbf{k}_3$  remain unchanged. With the limited number of reflections (33) collected at  $T = 2.7$  K in the present experiment, it was not possible to reliably solve the magnetic structure. It would also be worthwhile to trace the temperature dependence of the intensities for selected reflections with contrasting behaviors in the temperature range of interest.

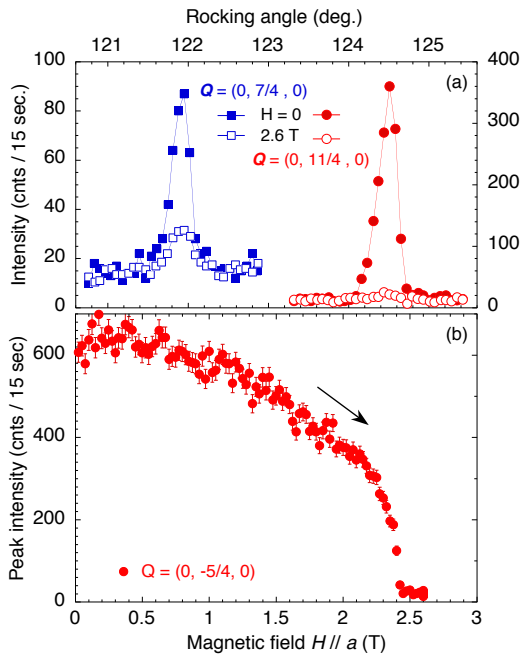


FIG. 9. (Color online) (a) Rocking curves through the  $020^-$  and  $030^-$  magnetic satellites at  $T = 1.7$  K for  $H_{\parallel a} = 0$  and 2.6 T. (b) Variation of the peak intensity of the  $010^-$  magnetic satellite [ $\mathbf{Q} = (0, -\frac{5}{4}, 0)$ ] in a magnetic field  $H \parallel a$  at  $T = 1.6$  K.

#### D. Magnetic field effects

Single-counter measurements have been performed in magnetic fields of up to  $H = 2.6$  T applied along the  $a$  axis (parallel to the ordered Nd moments). The peak intensity  $I_{010^-}$  of the  $\mathbf{Q} = (0, -\frac{5}{4}, 0)$  magnetic satellite was traced in an increasing magnetic field at  $T = 1.7$  K [Fig. 9(b)]. One observes a steady decrease, with the intensity dropping to zero at about 2.45 T. In their magnetization measurements, Kunimori *et al.*,<sup>7</sup> observed a steplike increase in  $M(H)$  at  $T = 1.4$  K for  $H \parallel a$ , at a transition field of  $H_c = 2.45$  T, in agreement with the present data.

Integrated intensities were measured for a limited set of magnetic reflections in a field of 2.6 T. The data reveal that, while the magnetic signal associated with the  $\mathbf{k}_1$  wave vector becomes completely suppressed or barely detectable at this magnetic field for some of the satellites [ $010^-$  or  $030^-$ , see Fig. 9(a), right], as expected from the curve in Fig. 9(b), it remains sizable for others, such as  $020^-$  [Fig. 9(a), left]. This implies that the order achieved in this region retains a staggered component associated with the same wave vector as in zero field, and the fully-polarized state is not yet achieved.

#### IV. DISCUSSION AND CONCLUSION

In the previous sections, we have demonstrated that the ordered magnetic structures formed in  $\text{NdFe}_2\text{Al}_{10}$  below  $T_N = 3.9$  K are far less simple than the antiferromagnetic order with  $\mathbf{k} = (0, 1, 0)$  reported previously for  $\text{CeRu}_2\text{Al}_{10}$  and  $\text{CeOs}_2\text{Al}_{10}$ .<sup>8–10,22</sup> Depending whether the crystallographic space group is assumed to remain  $Cmcm$  or to undergo a (as yet undetected) symmetry lowering to a primitive orthorhombic unit cell, the order of the Nd moments can be described as either double- $\mathbf{k}$  ( $\mathbf{k}_1$  and  $\mathbf{k}_3 = 3\mathbf{k}_1$ ) or single- $\mathbf{k}$  ( $\mathbf{k}_1$  alone), with  $\mathbf{k}_1 = (0, \frac{1}{4}, 0)$ . At the base temperature of  $T_{\min} \approx 1.6 - 1.7$  K, the powder and single-crystal data can be consistently accounted for assuming a collinear ( $\mathbf{m}_{\text{Nd}} \parallel a$ ) structure with constant magnetic moments of  $\approx 1.75(4)\mu_B$  (NPD) or  $1.95(7)\mu_B$  (single-crystal diffraction), consistent with the value of  $1.91\mu_B$  expected for the  $\text{Nd}^{3+}$  CF doublet ground state derived in Ref. 7.

In intermetallic lanthanide compounds, couplings between  $4f$  magnetic moments are usually dominated by RKKY interactions, and the wave vector of the structure is thus sensitive to peculiarities of the Fermi surface, which are beyond the scope of this work. However, to try and quantify the competition between the 24 different constant-moment structures (Sect. III B) consistent with the  $\mathbf{k}_1$  (and  $\mathbf{k}_3$ ) wave vectors, one can calculate the corresponding exchange energies, assuming couplings extending to the third nearest neighbors (Fig. 3). The results show that the structure derived from the refinements is actually that which minimizes the energy ( $E = -8J_1 - 8J_2 + 8J_3$ ) in the case when all three couplings are AFM (defined here as  $J > 0$  for convenience) and satisfy  $J_1 > 2J_3$  (1), and  $J_2 > J_3$  (2). This condition is not unreasonable since the distance to the first neighbors is significantly shorter than that to the second and third neighbors.

It is easy to see in Fig. 3 that AFM couplings to the first and second neighbors ( $J_1$  and  $J_2$ ) can be simultaneously satisfied if the spin sequence (from left to right) is changed to “+ + - - + + - -”, i.e. blue and red moments up, yellow and green moments down. This sequence actually corresponds to that observed in  $\text{CeRu}_2\text{Al}_{10}$  and  $\text{CeOs}_2\text{Al}_{10}$  (except for the Ce moments oriented parallel to  $c$ ), and it can be described in the  $Cmcm$  space group by the simple wave vector  $(0, 1, 0)$ . In this structure, all third-neighbor pairs are ferromagnetic (FM) and, in Ref. 11, magnetic excitation spectra of  $\text{CeRu}_2\text{Al}_{10}$  in the AFM state could be reproduced assuming exchange interactions with  $J_1$  (predominant and anisotropic) and  $J_2$  AFM, and  $J_3$  FM. It can be noted that, in the  $\text{YbFe}_2\text{Al}_{10}$  structure, there is one transition-metal atom lying between third-neighbor rare-earth ions, which can explain why  $J_3$  can change significantly from one compound to another. In  $\text{TbFe}_2\text{Al}_{10}$ , Reehuis *et al.*<sup>23</sup> have observed a commensurate magnetic structure below  $T = 11$  K, with cell dimensions  $a \times 5b \times c$ , which results from the squaring of the sine-wave modulation of the Tb moments appear-

ing at  $T_N$ . This structure is quite similar to that found in the present compound, apart from the change in the period along  $b$  from 4 to 5 unit cells.

The structure determined above for  $\text{NdFe}_2\text{Al}_{10}$  suggests that  $J_3$  is now AFM. It can be obtained from the  $\mathbf{k} = (0, 1, 0)$  structure by flipping a block of 8 consecutive magnetic planes in the original “...+)(+ -)(- +)(+ -)(- +)(+ -)(- +)(- ...” stacking (brackets denote near-neighbor AFM pairs strongly coupled by  $J_1$ ), to get “...+)(+ -) | (+ -)(- +)(+ -)(- +) | (- +)(+ -)(- ...” (vertical bars delimit the reversed range). The new sequence is identical to that shown in Fig 3. If one denotes the near-neighbor AFM pairs (forming alternating zigzag chains along  $c$ ) as  $A \equiv “+ -”$  and  $B \equiv “- +”$ , it is clear that the change from ABABABAB to A|ABAB|BAB can be described as the appearance of discommensurations. Similarly, the structure found in  $\text{TbFe}_2\text{Al}_{10}$  can be written as A|ABABA|ABAB, i.e. with a longer interval between discommensurations. Such steplike reversals of the moment direction reflect the constraint imposed on the system by the strong  $J_1$  couplings, which prevent it from adapting smoothly to a change in the wave vector of the interactions.

At the borders of one flipped block,  $J_2$  couplings become frustrated (FM), whereas initially FM  $J_3$  pairs become AFM. Correspondingly, the exchange energy  $E$  changes from  $-8J_1 - 16J_2 + 16J_3$  to  $-8J_1 - 8J_2 + 8J_3$ , and the spin reversal will thus produce a more stable structure only if  $J_3$  is larger than  $J_2$ . This, unfortunately, is in contradiction to condition (2) above. Therefore, while the comparison of exchange energies provides a hint as to why this particular  $\{\mathbf{k}_1, \mathbf{k}_3\}$  structure occurs rather than another, it cannot explain *simultaneously* why a  $\{\mathbf{k}_1, \mathbf{k}_3\}$  structure occurs in the first place, rather than  $\mathbf{k} = (0, 1, 0)$  anti ferromagnetism as in  $\text{CeRu}_2\text{Al}_{10}$ . A more realistic model, e.g. taking into account more distant neighbors and/or anisotropic couplings, is necessary to solve this problem.

The existence of a second phase transition below  $T_N$ , at about 2.5 K, is supported, in the present experiments, by the redistribution of intensities amongst magnetic satellites observed between 1.7 and 2.7 K (wave vector unchanged), but the exact structure formed in the intermediate temperature range remains to be determined precisely. Concerning the effect of a magnetic field at the

lowest temperature, the jump at  $H_c = 2.45$  T in the magnetic isotherm reported in Ref. 7 leads to an intermediate magnetic phase in which some satellites associated with the  $(0, \frac{1}{4}, 0)$  wave vector, in particular  $020^-$ , retain finite intensities at 2.6 T. A similar situation has been reported previously for  $\text{TbFe}_2\text{Al}_{10}$ , where a magnetic transition occurring at 0.8 T was interpreted as a spin-flip process, due to the large magnetocrystalline anisotropy, whereby some of the first-neighbor pairs switched from AFM to FM (Fig. 4 in Ref. 23). In that case, however, a second, metamagneticlike, transition from this ferrimagnetic state to the fully-polarized state took place at a higher field of 1.8 T. In  $\text{NdFe}_2\text{Al}_{10}$ , the magnetic isotherm exhibits a shoulder above the transition at  $H_c$ , finally reaching saturation, with a weak final slope, above 4 T.<sup>7</sup> This behavior suggests a different mechanism, possibly of the spin-flop type. The fact that the intensity of the  $020^-$  reflection does not vanish above  $H_c$  implies that the moments cannot be oriented along  $b$  (only magnetic components perpendicular to the scattering vector  $\mathbf{Q} \parallel b$  contribute to the neutron signal), a rather natural result since  $b$  is the hard anisotropy axis, according to magnetization data.<sup>7</sup> Additional measurements are needed to ascertain the direction of the AFM component in this state, but the  $c$  direction seems the most plausible.

Finally, the contrast between the commensurate order occurring in  $\text{NdFe}_2\text{Al}_{10}$  or  $\text{TbFe}_2\text{Al}_{10}$  and the simple AFM one found previously in their cerium-ruthenium and cerium-osmium homologues can be explained by relatively minor changes in the magnitude of the exchange interactions, in particular the coupling  $J_3$  between third neighbors. However, this similarity may be deceiving because the microscopic description of the Ce compounds has been argued to involve a prominent role of anisotropic  $c$ - $f$  hybridization, with a strong feedback on the magnitude and anisotropy of exchange interactions..

## ACKNOWLEDGMENTS

We are grateful to J.-L. Meuriot, Th. Robillard, J. Dupont, and X. Guillou for technical support during the experiments. K. S. was supported by a *Japan Society for the Promotion of Science* Research Fellowship.

\* Present address: Institute of Materials Structure Science, KEK, 1-1 Oho, Tsukuba, Ibaraki 305-0801, Japan

† e-mail address: jean-michel.mignot@cea.fr

<sup>1</sup> Y. Muro, K. Motoya, Y. Saiga, and T. Takabatake, J. Phys. Soc. Jpn. **78**, 083707 (2009).

<sup>2</sup> T. Nishioka, Y. Kawamura, T. Takesaka, R. Kobayashi, H. Kato, M. Matsumura, K. Kodama, K. Matsubayashi, and Y. Uwatoko, J. Phys. Soc. Jpn. **78**, 123705 (2009).

<sup>3</sup> A. M. Strydom, Physica B **404**, 2981 (2009).

<sup>4</sup> A. Kondo, J. Wang, K. Kindo, Y. Ogane, Y. Kawamura,

S. Tanimoto, T. Nishioka, D. Tanaka, H. Tanida, and M. Sera, Phys. Rev. B **83**, 180415 (2011).

<sup>5</sup> H. Tanida, Y. Nonaka, D. Tanaka, M. Sera, Y. Kawamura, Y. Uwatoko, T. Nishioka, and M. Matsumura, Phys. Rev. B **85**, 205208 (2012).

<sup>6</sup> R. Kobayashi, Y. Kawamura, T. Nishioka, H. Kato, M. Matsumura, K. Kodama, H. Tanida, M. Sera, K. Matsubayashi, and Y. Uwatoko, J. Phys. Soc. Jpn. Suppl. **80SA**, SA044 (2011).

<sup>7</sup> K. Kunimori, M. Nakamura, H. Nohara, H. Tanida,

- M. Sera, T. Nishioka, and M. Matsumura, *Phys. Rev. B* **86**, 245106 (2012).
- <sup>8</sup> J. Robert, J.-M. Mignot, G. André, T. Nishioka, R. Kobayashi, M. Matsumura, H. Tanida, D. Tanaka, and M. Sera, *Phys. Rev. B* **82**, 100404(R) (2010).
- <sup>9</sup> D. D. Khalyavin, A. D. Hillier, D. T. Adroja, A. M. Strydom, P. Manuel, L. C. Chapon, P. Peratheepan, K. Knight, P. Deen, C. Ritter, Y. Muro, and T. Takabatake, *Phys. Rev. B* **82**, 100405(R) (2010).
- <sup>10</sup> J.-M. Mignot, J. Robert, G. André, A. M. Bataille, T. Nishioka, R. Kobayashi, M. Matsumura, H. Tanida, D. Tanaka, and M. Sera, *J. Phys. Soc. Jpn. Suppl.* **80SA**, SA022 (2011).
- <sup>11</sup> J. Robert, J.-M. Mignot, S. Petit, P. Steffens, T. Nishioka, R. Kobayashi, M. Matsumura, H. Tanida, D. Tanaka, and M. Sera, *Phys. Rev. Lett.* **109**, 267208 (2012).
- <sup>12</sup> M. Sera, D. Tanaka, H. Tanida, C. Moriyoshi, M. Ogawa, Y. Kuroiwa, T. Nishioka, M. Matsumura, J. Kim, S. Tsuji, and M. Takata, *J. Phys. Soc. Jpn.* **82**, 024603 (2013).
- <sup>13</sup> J. Rodriguez-Carvajal, *Physica B* **192**, 55 (1993).
- <sup>14</sup> J. Rodriguez-Carvajal, *Commission on Powder Diffraction (IUCr) Newsletter* **26**, 12 (2001).
- <sup>15</sup> V. F. Sears, *Neutron News* **3**, 26 (1992).
- <sup>16</sup> A. Freeman and J. Desclaux, *J. Magn. Magn. Mater.* **12**, 11 (1979).
- <sup>17</sup> A. Gukasov, A. Goujon, J.-L. Meuriot, C. Person, G. Exil, and G. Koskas, *Physica B: Condensed Matter* **397**, 131 (2007).
- <sup>18</sup> J. Brown and J. Matthewman, *Cambridge Crystallography Subroutine Library*, Report No. RAL93-009 (1993).
- <sup>19</sup> V. M. T. Thiede, T. Ebel, and W. Jeitschko, *J. Mater. Chem.* **8**, 125 (1998).
- <sup>20</sup> D. T. Adroja, A. D. Hillier, Y. Muro, T. Takabatake, A. M. Strydom, A. Bhattacharyya, A. Daoud-Aladin, and J. W. Taylor, *Physica Scripta* **88**, 068505 (2013).
- <sup>21</sup> T. Hiroshi *et al.*, (2014), unpublished.
- <sup>22</sup> H. Kato, R. Kobayashi, T. Takesaka, T. Nishioka, M. Matsumura, K. Kaneko, and N. Metoki, *Journal of the Physical Society of Japan Supplement* **80**, 073701 (2011).
- <sup>23</sup> M. Reehuis, M. W. Wolff, A. Krimmel, E.-W. Scheidt, N. St sser, A. Loidl, and W. Jeitschko, *Journal of Physics: Condensed Matter* **15**, 1773 (2003).